SCIENTIFIC REP🅞RTS

OPEN

Radiopaque Fully Degradable Nanocomposites for Coronary Stents

Hui Ying Ang[1], Daniel Toong[2], Wei Shoon Chow[2], Welly Seisilya[2], Wei Wu[3], Philip Wong[1], Subbu S. Venkatraman [ID][2], Nicolas Foin[1,4] & Yingying Huang[2]

Bioresorbable scaffolds (BRS) were introduced to overcome limitations of current metallic drug-eluting stents and poly-L-lactide (PLLA) has been used in the fabrication of BRS due to its biodegradability and biocompatibility. However, such polymers have weaker mechanical properties as compared to metals, limiting their use in BRS. We hypothesized that nanofillers can be used to enhance the mechanical properties considerably in PLLA. To this end, polymer-matrix composites consisting of PLLA reinforced with 5–20 wt% barium sulfate ($BaSO_4$) nanofillers as a potential BRS material was evaluated. Stearic-acid (SA) modified $BaSO_4$ nanofillers were used to examine the effect of functionalization. Rigid nanofillers improved the tensile modulus and strength of PLLA (60% and 110% respectively), while the use of SA-$BaSO_4$ caused a significant increase (~110%) in the elongation at break. Enhancement in mechanical properties is attributed to functionalization which decreased the agglomeration of the nanofillers and improved dispersion. The nanocomposites were also radiopaque. Finite element analysis (FEA) showed that scaffold fabricated from the novel nanocomposite material has improved scaffolding ability, specifically that the strut thickness could be decreased compared to the conventional PLLA scaffold. In conclusion, $BaSO_4$/PLLA-based nanocomposites could potentially be used as materials for BRS with improved mechanical and radiopaque properties.

Current metallic drug-eluting stents (DES) have thin struts with biocompatible polymer coating, making them the first choice device for the treatment of coronary artery disease. However, the caging of the vessel permanently with a metallic implant runs the risk of impairing endothelial function and decreasing positive lumen remodeling. Clinical observations from several large-scale DES registries have revealed the occurrence of late adverse events that questions the safety of DES. Hence, bioresorbable scaffolds/stents (BRS) present an attractive alternative to DES by providing the temporal support and be resorbed in due time, allowing the vessel to return to a more natural and healed state[1,2].

Conceptually, the BRS is supposed to retain sufficient radial strength after implantation to prevent vessel recoil and to release the antiproliferative drug. After the healing period, the BRS is no longer required and should degrade to be resorbed completely, leaving the vessel with a healthy endothelium and normal vasomotion. BRS fabricated from bioresorbable polymeric materials are, in theory, more flexible and conformable and would influence the shear stress pattern to a lesser degree compared to a metallic DES[3,4]. The absence of any residual foreign material and restoration of endothelial coverage would also reduce the need for long-term dual antiplatelet treatment thereby decreasing the risk of bleeding. The resorption of the BRS would allow future intervention at the same site and facilitate the access to side branches that were jailed by the original stent[5,6]. Current BRS are either polymer-based (e.g. Poly-L-lactide, Polycarbonate) or metallic-based (e.g. Magnesium alloy).

Poly-L-lactide (PLLA) is a biodegradable, biocompatible and biologically inert synthetic polymer used widely in biomedical application such as tissue engineering scaffolds. PLLA-based BRS include ABSORB Bioresorbable Vascular Scaffold (BVS) (Abbott Vascular), DESolve (Elixir Medical), FORTITUDE/APTITUDE/MAGNITUTDE (Amaranth), ArterioSorb (Arterius), MIRAGE (Manli Cardiology), ART bioresorbable scaffolds (Arterial Remodeling Technologies). Biotronik's Magmaris is the only resorbable metallic BRS with a CE mark[1].

[1]National Heart Centre Singapore, 5 Hospital Drive, 169609, Singapore, Singapore. [2]School of Materials Science and Engineering, Nanyang Technological University, Nanyang Avenue, 639798, Singapore, Singapore. [3]Department of Mechanical Engineering, University of Texas at San Antonio, 1 UTSA Circle, San Antonio, TX, 78249, USA. [4]Duke-NUS Medical School, 8 College Road, 169857, Singapore, Singapore. Correspondence and requests for materials should be addressed to Y.H. (email: yingyinghuang@ntu.edu.sg)

PLLA has been widely studied as a biomaterial for several biomedical engineering applications due to its bio-degradability and biocompatibility[7–9]. Particularly, PLLA has been investigated widely as a choice of material in BRS fabrication[10]. Unprocessed PLLA will typically exhibit approximately 100-fold lower tensile modulus than cobalt or stainless steel which are the conventional materials used in DES. As a consequence of the lower modulus (both tensile and compressive), BRS fabricated from these bioresorbable materials may require up to 240% thicker struts in order to match the radial strength of the current metallic DES, thereby affecting the device's deliverability[11].

Polymeric devices also have a limit of expansion and can fracture due to over-dilation. It is important to improve the expandability of the BRS while maintaining radial strength[12]. With lesser strength, BRS requires extensive vessel preparation and may achieve lesser acute gain (defined as the difference between pre-procedural minimal luminal diameter, MLD, and immediate post-procedural MLD) than a metallic stent. Current PLLA devices also lack radiopacity, making the visualization and assessment of scaffold expansion difficult[1,13].

Nanocomposite polymeric materials present a novel class of materials with important properties in several engineering and biomedical applications. A polymeric nanocomposite comprises nanofillers dispersed within a polymer matrix. The concept of a nanocomposite material capitalizes on the inherent properties of the base polymer while enhancing the functionality of the composite device by the addition of nanofillers[14,15]. The nano-fillers are able to render additional features to the polymer that are usually not available in polymeric materials such as optical, electrical and mechanical properties[16–18]. In the field of biomaterials, the reinforcement effect of rigid nanofillers on polymers' mechanical properties is of particular interest. Nanofillers possess a large surface to volume ratio that increases the number of particle-matrix interactions when dispersed in a polymer and can improve the overall material properties[19–22]. The presence of the filler can reinforce the mechanical strength of the polymer by: (i) substituting the softer polymer matrix by a stiffer filler, (ii) immobilizing the polymer molecules on filler particle surfaces as a result of filler–polymer interaction, and (iii) stress transfer from the matrix to the filler[23]. The nanofillers can help to absorb energy from the applied stress and disperse it about a larger volume of the nanocomposite material, thereby improving the composite's properties[24,25].

The reinforcement effect of the nanofillers on the nanocomposite properties depends not just on the nature of fillers and polymer but also on the filler size, filler-polymer interfacial interaction and particle loading. It is well documented that the major challenge in fabricating nanocomposites is achieving a uniform dispersion and good integration of the nanofillers in the polymer matrix[26–28]. Most of the polymers are hydrophobic and incompatible with the hydrophilic nanofillers. The issue of nanofiller agglomeration and weak particle-polymer affinity often lead to detrimental effects on the mechanical strength[29–31]. The interactions between the polymer and filler at the interface significantly influence the composite's mechanical properties. Interfacial debonding is commonly the first step of failure and a lack of adhesion between the two phases will lead to phase separation and early material failure[32]. In the same way, a strong interfacial bonding between the nanofillers and polymer leads to an effective transfer of load from the matrix to the nanofillers, enhancing the composite's strength.

To achieve good interfacial adhesion between the fillers and polymer matrix, functionalization is often utilized to improve the particle-polymer affinity. Functionalization of the nanofillers can help to establish favorable interactions that prevent agglomeration of the fillers and improve the overall distribution of the fillers within the polymer matrix[33–35]. One method to functionalize the nanofillers is to covalently graft another suitable compound such as a surfactant to the surface of the fillers before addition to the polymer and this has yielded positive mechanical outcomes for bone cement applications[36,37].

In this study, we hypothesize that the use of PLLA reinforced by the addition of inorganic nanofillers such as barium sulfate ($BaSO_4$) can potentially overcome the drawbacks of current PLLA as a load-bearing biomaterial. $BaSO_4$ has been used extensively as a radiocontrast agent in X-ray imaging and other diagnostic procedures. Several studies have demonstrated the reinforcement and radiopaque properties of $BaSO_4$ in polymeric materials. Stearic acid was selected as a functionalizing agent due to its surfactant properties, enabling it to be conjugated to the inorganic fillers while forming targeted hydrophobic interaction with PLLA[38,39]. Hence in this study, we have formulated a nanocomposite material based on inorganic $BaSO_4$ nanofillers and PLLA, and studied the effect of loading and functionalization on the mechanical properties of PLLA. Finite Element Analysis (FEA) was also carried out to evaluate the effect of the materials using a generic stent design, and the nanocomposite material was employed to improve the scaffolding while reducing the stent thickness potentially.

Results

Effect of filler loading on nanocomposite mechanical properties.
The addition of non-functionalized $BaSO_4$ nanofillers in PLLA has a significant effect on the polymer tensile properties (Fig. 1). As seen from Fig. 1a,b, as the amount of nanofillers increased from 0% to 15%, the modulus and ultimate strength of the material increased, thereby demonstrating the mechanical reinforcement effect of the rigid nanofillers. However, further increment in $BaSO_4$ loading to 20% caused a significant decrease in the modulus and strength ($p < 0.05$). The optimal reinforcement results occurred at 15% $BaSO_4$ loading with a 62% and 300% increase in tensile modulus and strength respectively. The presence of the $BaSO_4$ nanoparticles caused a significant decrease in the material's elongation at break across all filler loadings.

Tensile Modulus. It has been reported that the tensile modulus of polymers can be improved by adding nanofillers since rigid inorganic particles are much stiffer than polymer matrices. Two models that predict the reinforcing effect of fillers on the matrix have been used in this study to correlate the experimental observations and the reinforcement effect of the nanofillers. The Guth's equation (Equation 1), which is a modified version of Einstein's equation was employed[40]:
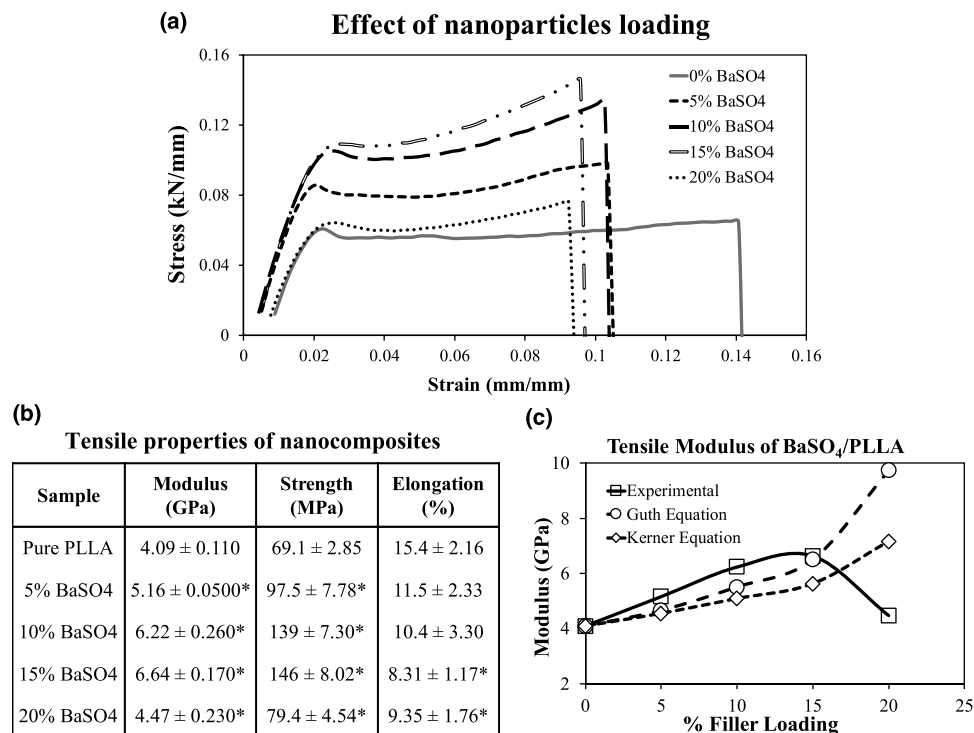
(a)

Effect of nanoparticles loading

(b)

Tensile properties of nanocomposites

Sample	Modulus (GPa)	Strength (MPa)	Elongation (%)
Pure PLLA	4.09 ± 0.110	69.1 ± 2.85	15.4 ± 2.16
5% BaSO4	5.16 ± 0.0500*	97.5 ± 7.78*	11.5 ± 2.33
10% BaSO4	6.22 ± 0.260*	139 ± 7.30*	10.4 ± 3.30
15% BaSO4	6.64 ± 0.170*	146 ± 8.02*	8.31 ± 1.17*
20% BaSO4	4.47 ± 0.230*	79.4 ± 4.54*	9.35 ± 1.76*

(c)

Tensile Modulus of BaSO$_4$/PLLA

Figure 1. Tensile properties of nanocomposite BaSO$_4$/PLLA fibers with different filler loadings (0–20%). (**a**) Representative stress-strain curve of the different nanocomposite samples. (**b**) Mean tensile modulus, strength and elongation at break of the nanocomposites are represented as mean value ± standard deviation. (n = 10) * indicates a statistically different value of the composite compared to the standard PLLA based on one-way ANOVA (p < 0.05). (**c**) The predicted tensile modulus of BaSO$_4$/PLLA nanocomposite as a function of filler loading according to Guth's equation and Kerner's equation[40,42].

$$E_c/E_m = 1 + 2.5\, V_p + 14.1 V_p^{\ 2} \tag{1}$$

where E_c and E_m are the tensile modulus of composite and matrix and V_p is the particle volume fraction (obtained based on the method described in Section 2.2). This equation is often used to estimate the effect of fillers on composite modulus as it incorporates: (1) a linear term reflects the stiffening effect of the fillers and (2) the second power term is the contribution of filler interaction, which is higher at increased filler loading[40,41]. According to Equation 1, increasing the particle volume fraction is expected to increase the modulus of the composite. Another model used to predict the effect of spherical nanofillers on composite material's modulus is the Kerner's equation (Equation 2)[42]:

$$E_c/E_m = 1 + V_p(1 - V_p)^{-1} \;*\; 15(1 - v_m)(8 - 10v_m)^{-1} \tag{2}$$

where v_m is the matrix Poisson ratio and taken to be 0.475 according to Soares *et al.*[43]. Figure 1c shows the estimated effect of nanofillers loading on the composite's modulus based on the two equations as compared to the experimental data.

From Fig. 1c, it is observed that BaSO$_4$ nanofillers have a reinforcement effect on the PLLA matrix, as increasing the filler loading (up till 15% by weight) increased the modulus. This improvement in modulus is in agreement with the modelling equations used. The results demonstrated that the Guth's model for predicting fillers effect on modulus is closer to the observed experimental data as compared to the Kerner's equation. However, both models do not predict a maximum in the modulus vs. volume fraction curve, which was observed experimentally here. The lesser fit of the Kerner's equation to the data can be attributed to its assumption that there is no interaction between particle–particle or matrix–particle, however, this will not be the case in the BaSO$_4$/PLLA system as seen in the agglomeration of the nanofillers[44].

Tensile Strength. Stress transfer between the fillers and the polymer affects the strength of the material. For nanocomposites with good interfacial adhesion, the applied stress can be transferred effectively from the polymer matrix to the fillers, which helps to improve the strength[41]. Nanofillers may also adversely affect the tensile strength of the composite material by acting as stress concentrators, due primarily to poor interfacial adhesion that results in poor or no stress transfer. There are many different equations and empirical models proposed to predict the effect of fillers on the composite tensile strength, but most models assume poor or no adhesion of nanofillers to matrix, which then predict a monotonic decrease in the composite strength with the addition of the
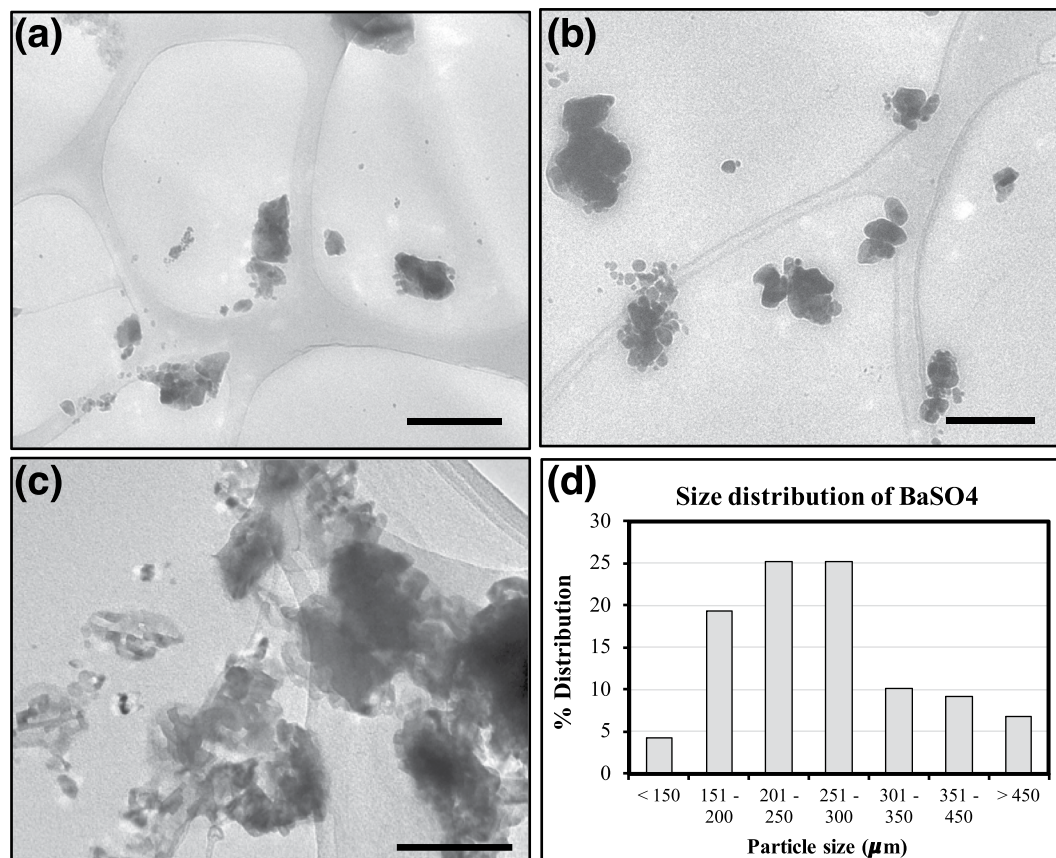
Figure 2. TEM images of BaSO4/PLLA nanocomposites with different filler loading at: (**a**) 5%, (**b**) 15% and (**c**) 20%. With increased filler loading, larger clusters of agglomerated $BaSO_4$ nanofillers are observed. Scale bar = 200 nm for all images. (**d**) Size distribution of the agglomerated $BaSO_4$ nanofillers based on n = 120 clusters/particles. The average particle size was $270 \pm 105\,\mu m$ in the 20% BaSO4/PLLA system.

fillers[45–47]. Interestingly, none of these models are applicable to this $BaSO_4$/PLLA nanocomposite system as the experimental data led to an increase in ultimate tensile strength with the addition of the fillers, passing through a maximum at 15% filler loading (similar to tensile modulus).

The increase in tensile strength of the composites upon the addition of the rigid fillers affirmed some form of adhesion between the nanofillers and the matrix. However, increasing the filler loading also led to an increased agglomeration of the fillers in the matrix, which could explain the decreased mechanical properties at 20% $BaSO_4$ loading. Nanosized fillers such as $BaSO_4$ have high surface energies, causing them to aggregate in order to lower the surface energies[48]. Such agglomeration is observed in the TEM images of the nanocomposite fibers with different $BaSO_4$ loading (Fig. 2). At the highest filler loading (20%), agglomeration is more prevalent as seen in Fig. 2c, leading to uneven distribution of fillers, which can result in phase separation, decreasing the mechanical properties. The size distribution of BaSO4 nanoparticles/clusters in the 20% $BaSO_4$/PLLA system is shown in Fig. 2d, more than 50% of the agglomerated the fillers were in the 200–300 μm size range. This observation has been reported in several other nanofillers/polymer composite studies[49–52].

Elongation at Break. The elongation at break of the nanocomposite material was significantly reduced when $BaSO_4$ nanofillers were added to PLLA across all filler loading, indicating a decrease in material ductility (Fig. 1). This significant decrease in elongation at break of the nanocomposite demonstrated that the fillers caused a reduction in polymer matrix deformation due to an introduction of mechanical restraints. It has been reported that at the microstructural level, the volume of the ductile polymer phase may be confined by the surrounding stiff nanofillers phase, which may constrain the local deformation under stress, thereby impairing the elongation at break[53,54]. This restraining effect has been observed in this $BaSO_4$/PLLA system. Hence, there appears to be a trade-off between the reinforcement effect and reduction in polymer's ductility when rigid $BaSO_4$ nanofillers were being introduced into PLLA.

Radiopacity. The results for radiopacity evaluation of the nanocomposites are shown in Fig. 3. It can be seen that PLLA (control) is completely radiolucent and not visible under x-ray imaging. The addition of both non-functionalized and functionalized $BaSO_4$ conferred radiopacity to the nanocomposite material (Fig. 3a) and the higher the filler loading, the higher the radiopacity value of the sample. From 5–15% filler loading, there were
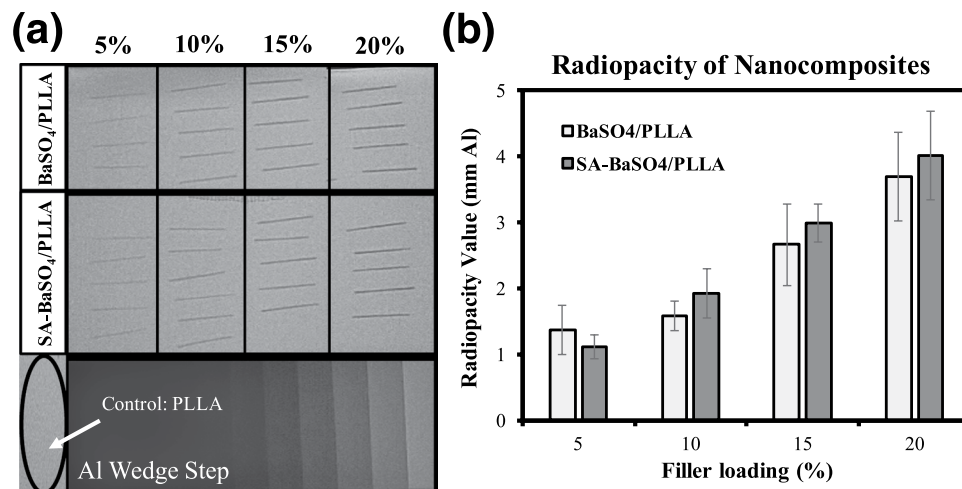
Figure 3. Radiopacity evaluation of the nanocomposites. (**a**) Digital radiographs of the nanocomposites with different filler loading, calibrated against the aluminum wedge step. (**b**) The radiopacity values of the samples expressed in mm Al. (n = 5 for each specimen). Error bar presents standard deviation.

no significant difference between the radiopacity values of composites with $BaSO_4$ or $SA-BaSO_4$ (p > 0.05). This result demonstrated that the nanocomposite formulation can be to fabricate implants that are radiopaque, making visualization (using radiography) during procedure possible.

Current BRS (with the exception of REVA Medical's FANTOM) have metallic (e.g. gold, platinum) radiopaque markers affixed onto the scaffold for visibility under x-ray. During scaffold deployment, the portion of a BRS with a marker may crack or stretch when stress is being applied, causing the markers to be dislodged in the process. A limitation of the current marker technology is that when viewed under fluoroscopy, the radiopaque markers do not provide good indication of scaffold expansion as they are usually only placed at the distal and proximal ends. During and after the procedure, the operator will not be able to assess scaffold expansion and lesion coverage accurately[1,55]. This also complicate retrieval in case of dislodgment of the scaffold from the delivery catheter. Hence, a material with adequate radiopacity can aid in addressing some of the imaging limitations of current polymeric BRS.

Effect of functionalization on nanocomposite mechanical properties.

In this study, conjugation of stearic acid (SA) (less than 1 wt% of the functionalized $BaSO_4$) to the surface of the nanoparticles had significant effect on the nanocomposite material as seen in the stress-strain curves (Fig. 4). In terms of modulus, functionalization did not affect the value significantly except at 15% loading (Fig. 4b). 15% filler loading gave the highest modulus for all the fillers-loaded PLLA, though the $SA-BaSO_4$/PLLA had a lower modulus compared to non-functionalized ones. As for tensile strength, using the $SA-BaSO_4$ resulted in higher strength at lower loading (<10%), after which the non-functionalized $BaSO_4$/PLLA gave significantly higher tensile strength (Fig. 4c). One interesting observation is that the $SA-BaSO_4$/PLLA nanocomposite material has significantly higher elongation at break across all the loading percentage, indicating an improvement in ductility compared to the non-functionalized system. $SA-BaSO_4$/PLLA nanocomposite at filler loading of 15% onwards has a marked improvement in elongation at break compared to pristine PLLA material (Fig. 4d).

Tensile Modulus. The slight decrease of $SA-BaSO_4$/PLLA modulus as compared to the non-functionalized $BaSO_4$/PLLA can be ascribed to the effect of stearic acid on the filler/matrix interlayer, though the effect was only relatively significant at 15% filler loading. This observation is in agreement with literature, demonstrating that the interaction of fillers with matrix do not influence tensile modulus significantly. Since tensile modulus was determined at low stress, in the linear part of the stress-strain curve, filler de-bonding has not yet occurred and hence should not be significantly affected by functionalization[56–58].

Tensile Strength. On the other hand, mechanical properties such as composite strength are more dependent on the interfacial interaction between fillers and matrix, thus warrants more discussion. The use of $SA-BaSO_4$ led to better tensile strength at lower loading (<10%) compared to non-functionalized fillers. As the content of filler increases, the amount of lubricating stearic acid is increased accordingly in the interlayer, which may lead to lower interfacial stress transfer efficiency. The presence of stearic acid can lead to a plasticizer effect on the composite system, thereby decreasing the modulus compared to non-functionalized nanocomposites. Stearic acid has been observed to act as a plasticizer during the melt compounding process, which decrease the modulus slightly but improved the elongation at break[59,60].

This plasticizer effect can be affirmed by the decrease in Tg and increased crystallinity of the functionalized $SA-BaSO_4$/PLLA system (Fig. 5). The DSC analysis showed that with the addition of the functionalized $SA-BaSO_4$ nanofillers, the decrease in Tg of the composite is significantly higher than that of the non-functionalized $BaSO_4$/PLLA (Fig. 5a). The decrease of Tg of a polymer is attributed to the additional free volume caused by the plasticizer, which aids in facilitating segmental movement[61,62]. Figure 5b shows the crystallinity of the composites at
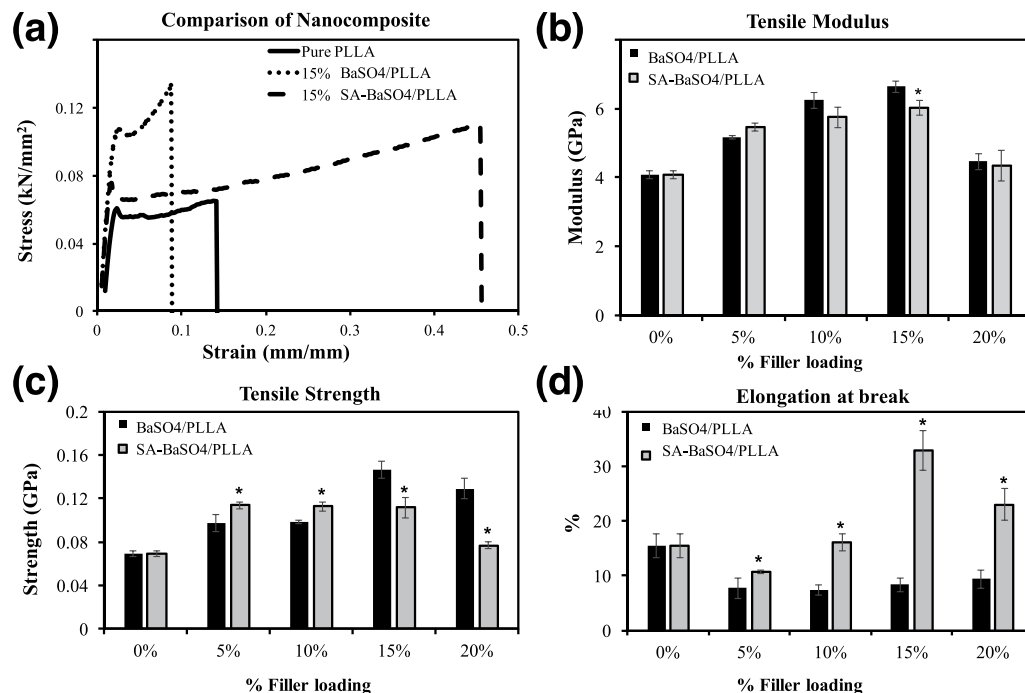
Figure 4. Tensile properties of non-functionalized $BaSO_4$ and $SA-BaSO_4$ filled PLLA. (**a**) Stress-strain curves of the pure PLLA and nanocomposite fibers. (**b–d**) Mean tensile modulus, strength and elongation at break of the nanocomposites. (n = 10) * indicates a statistically different value of the $SA-BaSO_4$/PLLA compared to the $BaSO_4$/PLLA at the same filler loading, based on one-way ANOVA (p < 0.05). Error bar presents standard deviation.

different loading and the $SA-BaSO_4$/PLLA have significantly higher crystallinity than non-functionalized $BaSO_4$/PLLA from 15% fillers loading onwards. This result suggested that without functionalization, the fillers do not function as effective nucleating agent and have likely hindered the mobility of the polymer chains as discussed earlier. This observation has been reported in several polymeric composite systems, especially for fillers with poor interfacial adhesion to the matrix or a high filler loading[63–66]. It can be concluded that functionalized $SA-BaSO_4$ had a plasticizer effect in PLLA.

To further examine the effect of filler loading on tensile strength of the composite, the strength of interfacial adhesion was estimated in this study using the following empirical equation by Pukanszky et al.[67]:

$$\sigma_c = \sigma_m \cdot (1 - V_p)(1 + 2.5V_p)^{-1} \cdot exp(BV_p) \tag{3}$$

where σ_c and σ_m refer to the tensile strength of the composite and matrix respectively, V_p is the volume fraction of the fillers and B is related to its relative loading bearing capacity, i.e. to the extent of reinforcement, which is dependent on interfacial adhesion. Rewriting Equation 3 into linear form yields Equation 4:

$$\ln\left[\sigma_c \cdot (1 + 2.5V_p) \cdot (1 - V_p)^{-1}\right] = \ln\sigma_m + BV_p \tag{4}$$

A graph of $\ln[\sigma_c \cdot (1 + 2.5V_p) \cdot (1 - V_p)^{-1}]$ vs. V_p was plotted (Fig. 5c) and resulted in a linear correlation, the gradient (B) of the plot is proportional to the strength of interaction. Based on the Fig. 5c, it can be observed that the non-functionalized $BaSO_4$ fillers (B = 8.40) had a slightly higher B value (dependent on interfacial adhesion) compared to $SA-BaSO_4$ (B = 8.03). This could account for the lower mechanical properties of $SA-BaSO_4$/PLLA compared to $BaSO_4$/PLLA at the same filler loading. Hence, the decrease in composite strength at higher $SA-BaSO_4$ loading could be due to the lubricating and plasticizing nature of stearic acid as mentioned earlier. The results agree with other mechanical studies on stearic acid functionalized nanofillers, where results have showed an improvement in filler dispersion due to lesser agglomeration but a reduced reinforcing effect of the fillers[31,38,39,68]. Experimental observations have demonstrated that the stearic acid modified filler did not improve the tensile modulus and strength of the polymers[69].

Elongation at Break. The significant improvement in elongation at break of the $SA-BaSO_4$/PLLA could be explained in terms of interfacial viscoelastic deformation and matrix yielding (Fig. 4d)[70]. Stearic-acid functionalized nanofillers have been reported to achieve improved dispersion state due to lesser agglomeration. Without functionalization, the nanofillers aggregate due to their van der Waals's bonding alignment and are expected to be in large clusters (Fig. 6a) within the polymer matrix. The interactions between the fillers cause a decrease in the inter-particulate distance [d] and result in clustering of the fillers. This leads to stronger inter-particulate
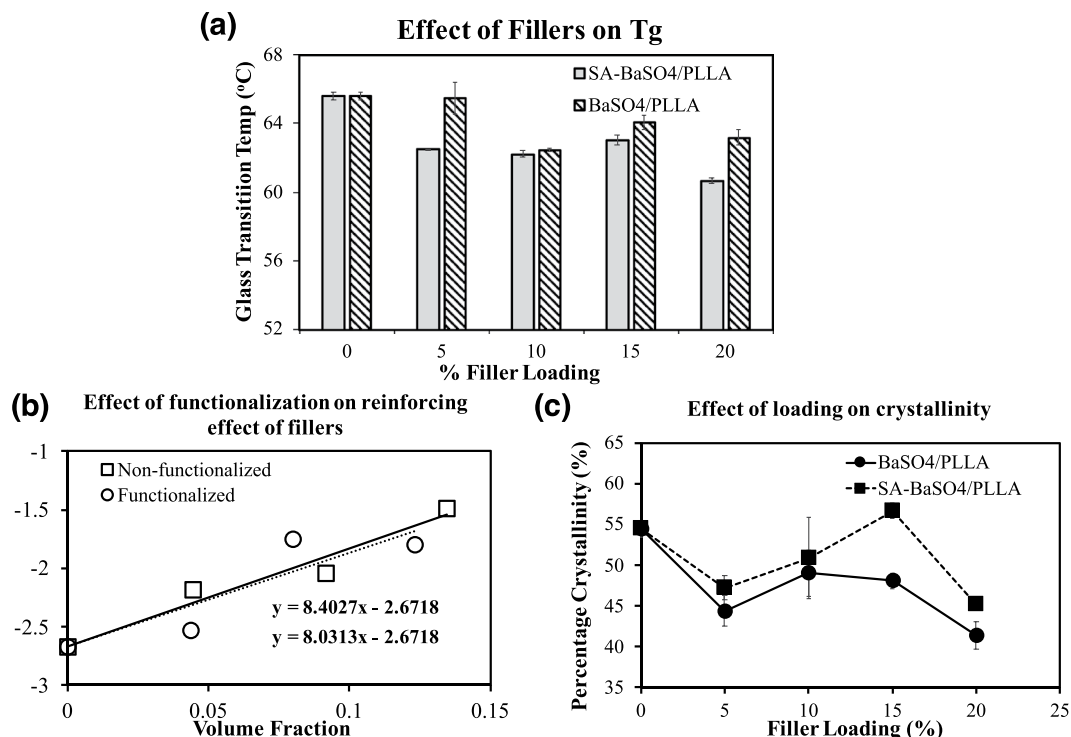
Figure 5. Effect of functionalization on nanocomposites based on DSC analysis and mathematical modeling. (**a**) Effect of filler loading on composite's Tg in both non-functionalized BaSO$_4$/PLLA and functionalized SA-BaSO$_4$/PLLA. (**b**) Crystallinity of BaSO$_4$/PLLA and functionalized SA-BaSO$_4$/PLLA at different filler loading. * indicates a statistically different value of the SA-BaSO$_4$/PLLA compared to the BaSO$_4$/PLLA at the same filler loading, based on one-way ANOVA ($p < 0.05$). Error bar presents standard deviation. (**c**) Effect of SA functionalization on the reinforcing effect of the filler in BaSO$_4$/PLLA composites, based on Equation 4. (The results for 20% filler loadings were omitted for both systems due to the decrease in tensile strength which were unable to be represented accurately by the mathematical models).
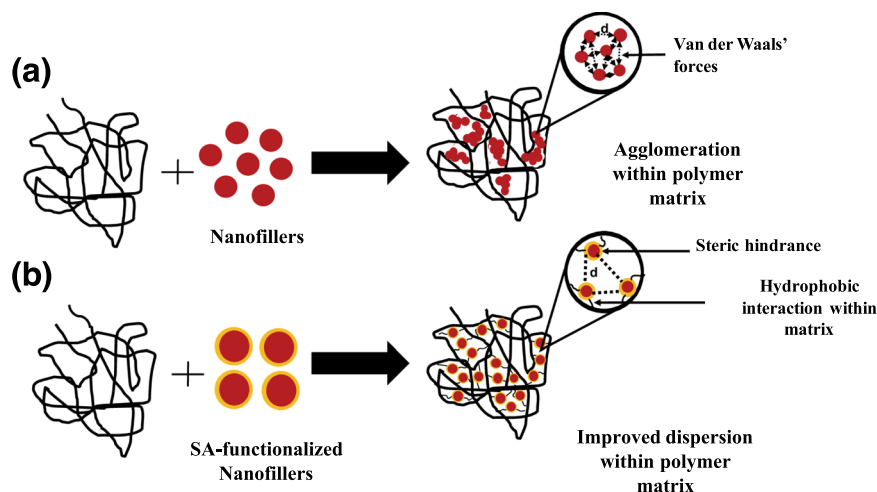

Figure 6. Schematic illustrating the effect of functionalization on filler dispersion in a polymer matrix. (**a**) Without functionalization, agglomeration of the nanofillers are evident due to high surface energies of the fillers. (**b**) With functionalization, targeted interactions can be established between the matrix and fillers, increasing the inter-particulate distance [d] and improving dispersion.

adhesion, keeping the structural integrity of the large aggregates during deformation. The presence and size of these aggregates causes a reduction in matrix deformation by acting as mechanical restraints, thereby decreasing the composite's ductility[53]. Rong *et al.* demonstrated that the decrease in ductility in the polymeric composite
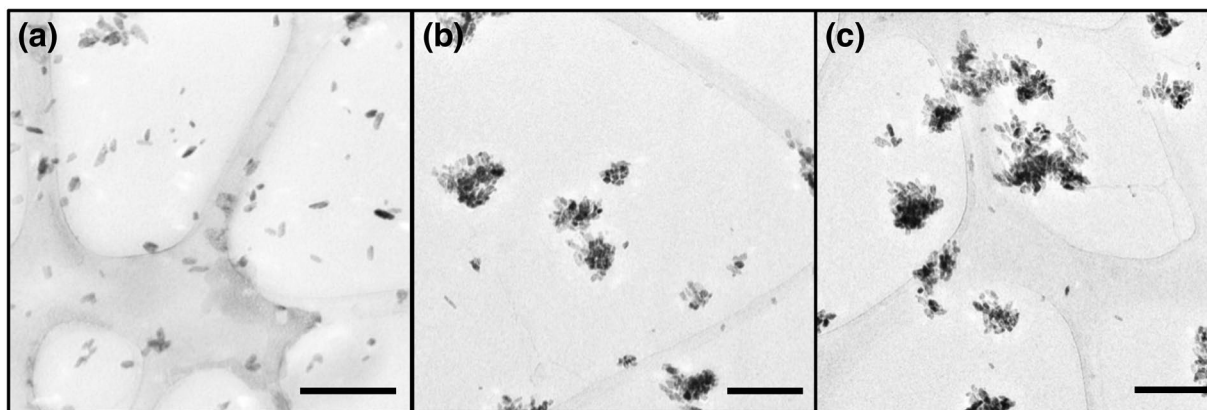
Figure 7. TEM images of the SA-BaSO$_4$/PLLA nanocomposites with different filler loading: (**a**) 5%, (**b**) 15% and (**c**) 20%. The agglomeration of the nanofillers are less severe and it is possible to identify individual particle. Magnification: Scale bar: 200 nm.

system suggested that matrix deformation is influenced by both interfacial interaction and dispersion state of the fillers. The decrease in ductility is found to be more pronounced at higher filler loading[20].

On the other hand, stearic acid functionalization caused weakened filler/filler interactions, favoring a dispersion of smaller aggregates within the polymer matrix, increased the inter-particulate distance (d) between fillers as shown in the schematic in Fig. 6b[56,71]. Weakened interactions amongst the fillers and a smaller aggregate size leads to an increase in the number of fillers taking part in the deformation of the material. These explanations can be supported by the TEM images in Fig. 7 whereby the SA-BaSO$_4$/PLLA had smaller clusters of fillers within the nanocomposites as compared to BaSO$_4$/PLLA at the same loading percentage (Fig. 2). It can be observed that the SA-BaSO$_4$ also exhibited aggregation at higher loading, reinforcing the detrimental effect of high filler loading on aggregation and mechanical properties. However, for the functionalized system, the resultant clusters are smaller in size and the fillers still maintained their distinct shape unlike the non-functionalized BaSO$_4$, which appeared in larger agglomerated clusters.

Functionalization of nanofillers can be done to: (i) increase the hydrophobicity of the hydrophilic fillers in order to facilitate filler/matrix miscibility due to increased interaction between the two, (ii) prevent agglomeration of the fillers by introducing repulsive forces and (iii) improve the interfacial adhesion between the filler and matrix, thereby promoting a more effective transfer of stress, increasing the strength of the composite. Based on the results in this section, it can be concluded that the use of stearic acid to functionalize BaSO$_4$ led to decreased agglomeration of the fillers but did not improve the interfacial adhesion between the filler and the polymer, which can be observed in the decrease in composite strength compared to the non-functionalized BaSO$_4$. This could be due to the short chain length of stearic acid, which is considered too short to be effectively entangled within the polymer matrix[47,72]. Furthermore, it has been reported that the use of surfactant such as stearic acid has the plasticizer effect which weakens interactions between the fillers and polymer thus facilitating interface debonding[73].

Finite Element Analysis (FEA). Simulation work was done to compare the scaffolding ability of the scaffolds fabricated using different materials. The strut thickness with the SA-BaSO$_4$/PLLA system was further modified with decreased thickness to evaluate the potential outcomes of using the nanocomposite material. The expansion and recoil of the 15% SA-BaSO$_4$/PLLA scaffold with the tube is shown in Fig. 8a,b, and the PLLA scaffold displayed similar deformation. The 15% BaSO$_4$/PLLA scaffold had several locations where the strain reached the elongation limit of the material during expansion, causing scaffold fractures as seen in Fig. 8c,d.

The averaged displacement of inner tube surface contacted with the scaffold is 0.16 mm for 15% SA-BaSO$_4$/PLLA and 0.08 mm for PLLA stent respectively. The peak MP strain that the 15% SA-BaSO$_4$/PLLA BRS experienced during expansion was 15.3% (Fig. 8d), which was far lesser than its elongation limit (Fig. 4d). 15% BaSO$_4$/PLLA BRS had lesser peak MP stain (13.9%) compared to the functionalized BRS and a similar strain distribution, but its peak strain is near to its the elongation limit. The expansion and scaffolding of the 15% SA-BaSO$_4$/PLLA BRS with reduced strut thickness (100 μm) is shown in Fig. 9a,b and the averaged tube displacement was 0.37 mm. During expansion, it had a peak MP stain of 24.9% (Fig. 9c), which is still below the elongation limit of the material.

To compare the influence of material properties on the BRS function, the FEA work evaluated three scenarios based on different stent materials and the results were aligned with the earlier mechanical testing outcomes. 15% BaSO$_4$/PLLA BRS experienced fracture due to the low ductility of the material. On the other hand, the PLLA BRS barely survived the scaffold expansion with a scaffolding ability just half of the 15%SA-BaSO$_4$/PLLA (considering the averaged displacement of inner tube surface contacting the scaffold).

Based on this simulation result, the 15% SA-BaSO$_4$/PLLA BRS demonstrated reliable structure integrity during expansion and better scaffolding ability than PLLA and 15% BaSO$_4$/PLLA. With enhanced material properties, the FEA data also showed that BRS fabricated from the functionalized nanocomposite material could potentially increase scaffolding by 130% (0.37 vs 0.16 mm) while reducing the thickness by 33% (0.1 vs 0.15 mm).
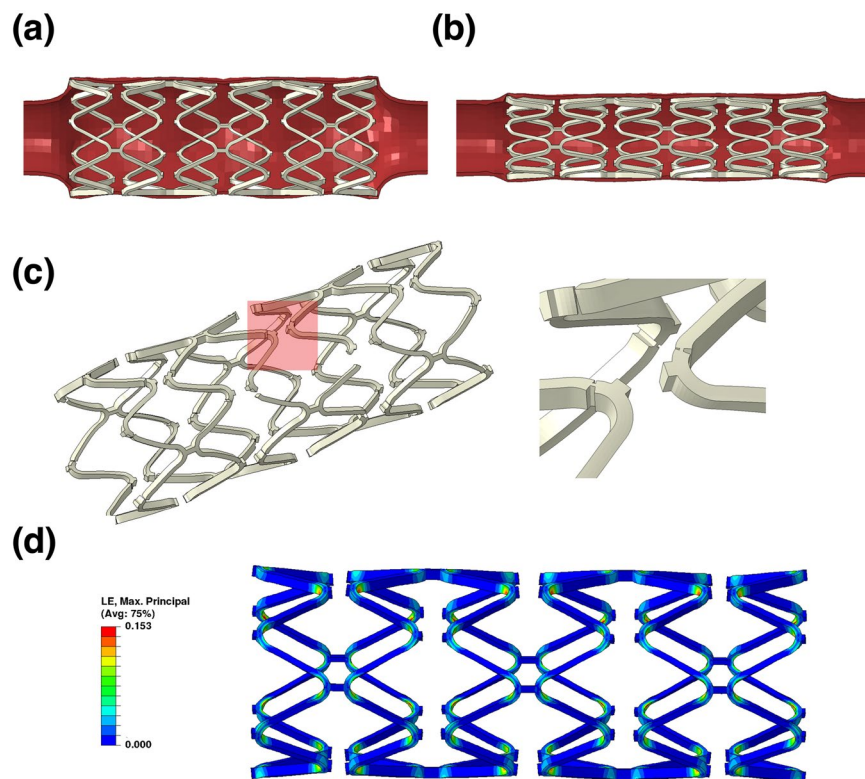
Figure 8. FEA of polymeric materials using a scaffold design with 150 μm strut thickness. (**a**) The expansion and (**b**) scaffolding of the 15% SA-BaSO$_4$/PLLA BRS. (**c**) Scaffold fracture happened to 15% BaSO$_4$/PLLA BRS during expansion and the marked part has been zoomed in to show the fractures. (**d**) The MP train contour of 15% SA-BaSO$_4$/PLLA BRS at maximum expansion (PLLA-based BRS has a similar MP train contour, hence is represented by the same figure here).
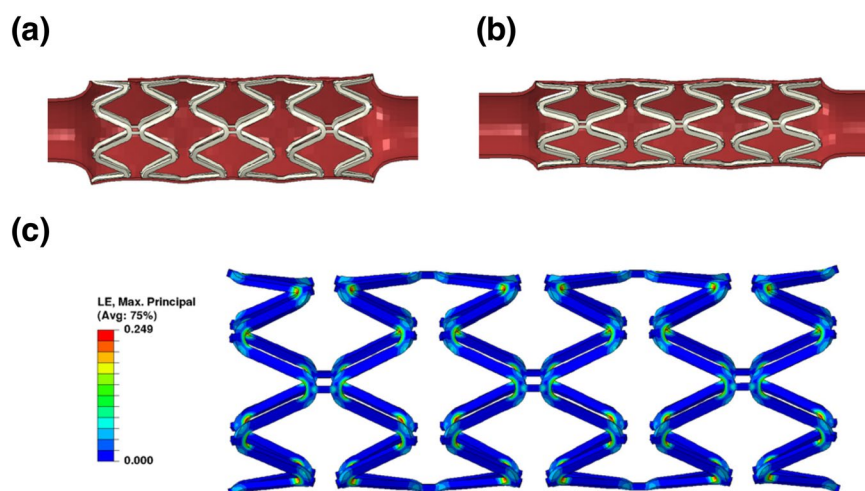

Figure 9. FEA of 15% SA-BaSO$_4$/PLLA BRS with 100 μm strut thickness. (**a**) Expansion, (**b**) Scaffolding and (**c**) strain contour at maximum expansion of BRS with reduced strut thickness.

Although the peak strain was increased by more than 60% (0.249 vs 0.153), the BRS still maintained its integrity and this could be attributed to the improved elongation limit of the SA-BaSO$_4$/PLLA system.

Following the clinical lessons learnt from the BVS studies, there has been a concerted drive towards minimizing strut thickness. The newer generation of BRS has moved away from the original 150 μm design and has gone to lower than 100 μm. Thinner struts decrease protrusion and improve embedment of the struts, hence is expected theoretically to contribute to less flow disturbance compared to the thick struts of the current BVS, and possibly better endothelialization. Studies have shown that thinner strut BRS has better embedment of struts and lesser

Sample	Nanoparticle	Filler Loading (%)
Control (PLLA)	No nanoparticles	—
BaSO$_4$/PLLA	Non-functionalized BaSO$_4$	5, 10, 15, 20
SA-BaSO$_4$/PLLA	Functionalized SA-BaSO$_4$	5, 10, 15, 20

Table 1. Formulations of different nanocomposite samples.

alteration of physiologic shear stress, thereby enhancing re-endothelialization[74,75]. The FEA work has provided important insights into the stress distribution and potential strut fractures of the BRS when deployed, and shown some of the potential mechanical advantages of the nanocomposite material in these aspects. This simulation can also aid in understanding the effect of strut thickness reduction on the expansion limit of the proposed nanocomposite materials.

Conclusion

The mechanical properties of a nanocomposite BaSO$_4$/PLLA material were modified using functionalization. The addition of rigid fillers such as nanosized BaSO$_4$ had a reinforcement effect on the polymer as evidenced by the increase in tensile modulus and strength of the material, but ductility is decreased. The optimized formulation (15% BaSO$_4$/PLLA) had an approximate 60% and 110% increase in tensile modulus and strength respectively, followed by 45% decrease in ductility. Functionalization of BaSO$_4$ with stearic acid was shown to have decrease the agglomeration of the nanofillers, thereby improving the elongation at break of the composite significantly. Functionalization did not increase the modulus and strength of SA-BaSO$_4$/PLLA as compared to BaSO$_4$/PLLA (p > 0.05). Stearic acid as functionalizing agent was found to exert a plasticizer effect on PLLA, as evidenced by the DSC data and mechanical characterization. The BaSO$_4$-filled composites were also radiopaque and could be visualized under x-ray. FEA demonstrated the potential benefit of using the nanocomposite material as a BRS candidate since the improved mechanical properties allowed for reduced strut thickness while maintaining structural support.

Future work will address some of the limitations of the current study in evaluating the material as a potential BRS candidate. For example, the nanocomposite material will be extruded into different thicknesses and laser-cut into a BRS prototype for further characterization such as radial testing and overexpansion evaluation. More FEA work will have to be conducted to evaluate other parameters such as different scaffold designs. The degradation rate and biocompatibility of the BRS will also need to be studied in order to understand its long-term behavior.

The use of polymeric composites reinforced with rigid fillers present an effective way to enhance the mechanical properties of the material for load-bearing devices. The fate and clearance of the fillers in the body after polymer degradation remains an area of scrutiny. BaSO$_4$ is considered a poorly soluble low toxicity particle and its "particokinetics" is influenced by the particle size and route of exposure[76]. While several studies have been conducted on the clearance and toxicity of inhaled and intravenous (IV) injected BaSO$_4$ nanoparticles, little data is available regarding the fate of implanted BaSO$_4$[77–79]. It was found that for injected BaSO$_4$ particles (~300 nm), fecal excretion was the dominant elimination pathway in a rat model. IV-injected BaSO$_4$ was studied to understand the fate of circulating BaSO$_4$ nanoparticles in the organs and it was demonstrated that a low concentration in the organs was achieved after 7 days in the animal model[77]. Previous work by Lämsä et al. had also explored the toxicity of a BaSO$_4$/PLA stent in a rat model, reporting no adverse effect after 21 days[80]. More work has to be done in this area to better understanding on the clearance of the BaSO$_4$ fillers after the degradation of the nanocomposite.

Presently, both the polymer-based and magnesium-based BRS platforms remain limited by their large profile and strut thickness, as compared to metallic DES. Research is being done to improve the properties of bioresorbable materials in order to reduce the strut thickness as seen from newer generation of BRS (e.g. Amaranth Medical's FORTITUDE and APTITUDE). In conclusion, BaSO$_4$/PLLA-based nanocomposites are good potential candidate materials for BRS with more desirable mechanical and radiopaque properties compared to PLLA alone.

Materials and Methods

Fabrication of nanocomposite polymeric material. PLLA (PURASORB PL inherent viscosity midpoint = 8 dl/g, Lot number: 0404002128) was purchased from Corbion (Netherlands) and employed as the base polymer. Non-functionalized BaSO$_4$ nanoparticles is a product of Nanoshel (USA). The formulation of different nanocomposite samples fabricated in this study is shown in Table 1. The samples were fabricated using a twin-screw (Xplore Micro 5cc) microcompounder (Netherlands) and the polymer resin and nanoparticles were compounded at a temperature of 190 °C for 7 minutes before extrusion. The extrudates were cut into granules and fed back to the compounder for a second round of mixing for 5 minutes before being extruded. The nanocomposite fibers obtained from the extrusion were 180 ± 10 μm and were used for further testing and characterization.

Transmission electron microscopy (TEM). TEM (Libra 120 Plus, Carl Zeiss, Germany) was employed to examine the dispersion of the nanoparticles within the nanocomposite material. The extruded composite fibers were embedded in araldite epoxy resin (Ted Pella, USA), cured at 60 °C for 24 hours and sectioned into 100 nm slices using ultramicrotomy. The slices were floated on a Formvar-coated copper TEM grid from deionized water and visualized using the TEM. The volume fraction of the nanocomposite material was determined from the automatic threshold method using Image J software. In this method, color-based thresholding was used to segment the fillers from the polymer matrix. The "Analyze" tool from the software will calculate the integrated
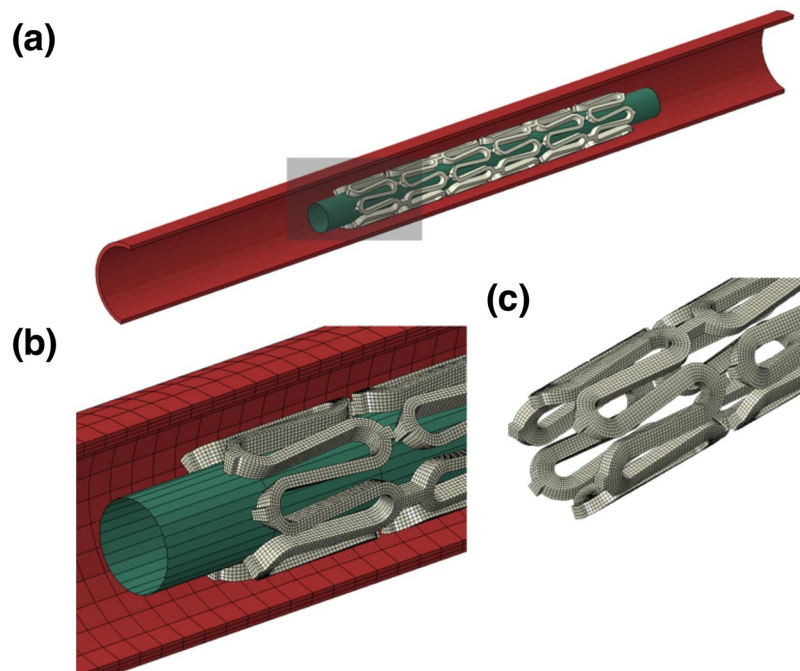
Figure 10. The FEA model employed in this study consists of a stent, a rigid balloon, and a silicon rubber tube (**a**) and the marked part was amplified to show the (**b**) meshing of the model and the (**c**) shape and meshing of the scaffold with reduced strut thickness.

densities (Area (No. of pixels) x Total Intensity of the pixels) of the different regions. This provides an estimation for the volume fraction of the fillers in the nanocomposite material. The volume fraction of the fillers is presented as an average of 10 TEM images per sample and 3 samples were used for each formulation. Image analysis was also performed using the same software to determine the size distribution of the agglomerated $BaSO_4$ nanoparticles within the PLLA matrix. A total of 120 nanoparticles were measured.

Differential scanning calorimetry (DSC).   A Perkin- Elmer DSC 8000 was used to study the thermal properties at a heating rate of 10 °C/min. The samples were cut into smaller pieces to improve contact with the sample pan. The Tg was determined as the point of half heat capacity extrapolated and the melting temperature (Tm) was determined as the peak temperature. The crystallinity of the material was calculated from the fusion enthalpy of melting (ΔH_m), which was obtained from the DSC melting curve. Based on literature, the theoretical heat fusion of 100% crystalline PLLA was employed to be 93.1 J/g. The crystallinity of the PLLA in this work was calculated by[81]:

$$\% \ \text{Crystallinity} = (\Delta H_m/93.1 \times W_p) \times 100\% \tag{5}$$

where ΔH_m is the enthalpy of fusion for the sample in J/g. an W_p is the weight fraction of PLLA in the composites. Triplicates were done for each sample to ascertain the reproducibility of the results.

Mechanical testing of nanocomposite polymeric material.   All nanocomposite materials were subjected to tensile testing using an MTS C42 Test System (MTS Systems, MN, USA). A 50 N load cell was used for the testing and all samples were pulled at a constant crosshead speed until failure. The extension rate was set at 0.1 mm/min and the stress-strain curves were obtained using the MTS software. The tensile modulus, the ultimate tensile strength (UTS) and elongation at break were obtained from the stress-strain curves. The values were averaged from 10 samples for each sample. The test specimens (nanocomposite fibers) were all standardized to be $180 \pm 10\,\mu m$ in diameter and 40 mm in length (for the testing length) after being mounted onto the MTS.

Radiopacity measurement.   For radiopacity evaluation, five samples per concentration (extruded fibers with 1.00 ± 0.05 mm in diameter and 20 ± 2 mm in length) were used. The samples were placed adjacent to a calibrated aluminium step wedge (Biomedia, Singapore) with 3.2-mm increments and imaged according to the adapted protocol[82]. A standard X-ray machine (Philips Clarity FD20) was used to irradiate X-rays onto the specimens using an exposure time of 4 ms at 76 mA and a cathode-target film distance of 100 cm. The tube voltage was set at 50 ± 5 kV. The radiographs were processed (AGFA Enterprise Imaging System), and a digital image of the radiograph was obtained. The grey pixel value on the radiograph, of each step in the step wedge was determined using an imaging programme, ImageJ (NIH, USA). Numbers between 0 and 255 with 0 representing pure black and 255 pure white were assigned accordingly. The equation of the trend line in the graph of aluminium thickness vs. grey pixel value can then be used to calculate the pixel value of a sample based on the sample thickness in mm of aluminium. The grey pixel values of the samples were computed ImageJ and the obtained equation to calculate the equivalent radiopacity expressed in mm of aluminium.

Statistical analysis. All mechanical tests were done in 10 repetitions for each type of nanocomposite samples and numerical data were analyzed using standard analysis of variance (ANOVA) technique and statistical significance was considered at $p < 0.05$.

Finite Element Analysis. In this study, the simulation involved the implantation of a scaffold into a silicon rubber tube to examine if the device can maintain its integrity during expansion. The whole model employed in this simulation is shown in Fig. 10a,b. The generic scaffold design has a length of 8 mm, an outer diameter of 1 mm, a thickness of 0.15 mm (150 μm) and strut width of 0.9 mm with six rings connected by two links in-between. The material properties of the three materials (PLLA, 15% $BaSO_4$/PLLA and 15% SA-$BaSO_4$/PLLA) were assigned to the scaffold model for three simulation scenarios.

The silicon rubber tube has a thickness of 0.1 mm, an inner diameter of 1.8 mm and a length of 20 cm (E = 1.5 MPa and v = 0.49). The rigid balloon has a diameter of 0.7 mm and a length of 10 mm. The modified scaffold design (Fig. 10c) has a thickness of 0.1 mm (100 μm) and width of 0.15 mm (the corresponding balloon has an increased diameter of 0.8 mm). The scaffold and tube model were meshed with hexahedral solid elements with rigid balloon surface elements. A sensitive analysis has been applied to ensure the elements density is enough. Two interactions, between the inner scaffold surface and rigid balloon, and between outer scaffold surface and inner tube surface, were established to simulate the contacts between scaffold and rigid balloon, and between scaffold and tube.

Quasi-static simulation was carried on using the finite element code ABAQUS/Explicit (Dassault Systèmes Simulia Corp., Providence, RI). In each of the four scenarios, the rigid balloon was expanded until the outer stent diameter reached 3 mm, followed by the recoiling of the balloon to its original shape, leaving the BRS supporting the tube by itself. For boundary conditions, the tube was fixed in all directions at its two ends and the rigid balloon can only expand and recoil in radial direction.

A material fracture mechanism was considered in the simulation to evaluate if the materials could endure the severe deformation during scaffold expansion. When the strain of a scaffold element reaches the elongation limit of the material assigned, the element will be considered as having failed, and therefore deleted from the model. For the scenarios without scaffold element failure, the averaged displacement of the inner tube surface contacted with the scaffold was calculated to evaluate the scaffolding ability of the scaffold; meanwhile, the maximum principal (MP) strain of the scaffold during expansion was also evaluated. As required by the FEA code, the strains applied in the simulation and shown in FEA results were true strains (logarithmic strains, LE).

Data Availability

The data that support the findings of this study are available within the paper.

References

1. Ang, H. Y. *et al*. Bioresorbable stents: Current and upcoming bioresorbable technologies. *Int J Cardiol* **228**, 931–939 (2017).
2. Bowen, P. K. *et al*. Biodegradable Metals for Cardiovascular Stents: from Clinical Concerns to Recent Zn-Alloys. *Advanced Healthcare Materials* **5**, 1121–1140 (2016).
3. Alfonso Lelasi, M. T. Current Status and Future Perspectives on Drug-eluting Bioresorbable Coronary Scaffolds: Will the Paradigm of PCI Shfit? *EMJ Int. Cardiol.* **1**, 81–90 (2014).
4. Garg, S. & Serruys, P. W. Coronary stents: looking forward. *J Am Coll Cardiol* **56**, S43–78 (2010).
5. Iqbal, J. *et al*. Bioresorbable scaffolds: rationale, current status, challenges, and future. *Eur Heart J* **35**, 765–76 (2014).
6. Neamtu, I. *et al*. Current concepts on cardiovascular stent devices. *Mini Rev Med Chem* **14**, 505–36 (2014).
7. Jeong, B., Bae, Y. H., Lee, D. S. & Kim, S. W. Biodegradable block copolymers as injectable drug-delivery systems. *Nature* **388**, 860–2 (1997).
8. Anderson, J. M. & Shive, M. S. Biodegradation and biocompatibility of PLA and PLGA microspheres. *Advanced Drug Delivery Reviews*, **64**, Supplement, 72–82 (2012).
9. Huang, Y., Ng, H. C., Ng, X. W. & Subbu, V. Drug-eluting biostable and erodible stents. *J Control Release* **193**, 188–201 (2014).
10. Xiong, G. M. *et al*. Materials technology in drug eluting balloons: Current and future perspectives. *J Control Release* **239**, 92–106 (2016).
11. Berglund, J., Guo, Y. & Wilcox, J. N. Challenges related to development of bioabsorbable vascular stents. *EuroIntervention*, **5** Suppl F, F72–9 (2009).
12. Ormiston, J. A., De Vroey, F., Serruys, P. W. & Webster, M. W. Bioresorbable polymeric vascular scaffolds: a cautionary tale. *Circ Cardiovasc Interv* **4**, 535–8 (2011).
13. Wang, Y. *et al*. A Nontoxic Additive to Introduce X-Ray Contrast into Poly(Lactic Acid). Implications for Transient Medical Implants Such as Bioresorbable Coronary Vascular Scaffolds. *Advanced Healthcare Materials* **3**, 290–299 (2014).
14. Islam, M. S., Masoodi, R. & Rostami, H. The Effect of Nanoparticles Percentage on Mechanical Behavior of Silica-Epoxy Nanocomposites. *Journal of Nanoscience* **2013**, 10 (2013).
15. Martínez de Arenaza, I., Sadaba, N., Larrañaga, A., Zuza, E. & Sarasua, J. R. High toughness biodegradable radiopaque composites based on polylactide and barium sulphate. *European Polymer Journal* **73**, 88–93 (2015).
16. Bunk, J. K. G. *et al*. Nanoparticle Distribution in Three-Layer Polymer–Nanoparticle Composite Films: Comparison of Experiment and Theory. *Particle & Particle Systems Characterization* **32**, 123–131 (2015).
17. Jayaraman, A. & Schweizer, K. S. Effective Interactions and Self-Assembly of Hybrid Polymer Grafted Nanoparticles in a Homopolymer Matrix. *Macromolecules* **42**, 8423–8434 (2009).
18. Tanahashi, M. Development of Fabrication Methods of Filler/Polymer Nanocomposites: With Focus on Simple Melt-Compounding-Based Approach without Surface Modification of Nanofillers. *Materials* **3**, 1593 (2010).
19. Mohammed, U. & Sun, C. T. Effect of Nanoparticle Dispersion on Mechanical Behavior of Polymer Nanocomposites. In *50th AIAA/ASME/ASCE/AHS/ASC Structures, Structural Dynamics, and Materials Conference*, ed: American Institute of Aeronautics and Astronautics, 2009.
20. Rong, M. Z. *et al*. Structure–property relationships of irradiation grafted nano-inorganic particle filled polypropylene composites. *Polymer* **42**, 167–183 (2001).
21. Njuguna, J., Pielichowski, K. & Desai, S. Nanofiller-reinforced polymer nanocomposites. *Polymers for Advanced Technologies* **19**, 947–959 (2008).
22. Yan-Hua, C. A. I. Effects of Barium Sulphate on Thermal Behaviour of Poly(L-lactic Acid). *Asian Journal of Chemistry* **25**, 2170–2172 (2013).

23. Kalfus, J. & Jancar, J. Reinforcing mechanisms in amorphous polymer nano-composites. *Composites Science and Technology* **68**, 3444–3447 (2008).

24. Haupert, F. & Wetzel, B. Reinforcement of Thermosetting Polymers by the Incorporation of Micro- and Nanoparticles. In *Polymer Composites: From Nano- to* Macro-Scale, ed Boston, MA: Springer US, pp. 45–62 (2005).

25. Schadler, L. S., Polymer-Based & Nanocomposites, P.-F. In *Nanocomposite Science and Technology*, ed: Wiley-VCH Verlag GmbH & Co. KGaA, pp. 77–153 (2004).

26. Kumar, S. K., Jouault, N., Benicewicz, B. & Neely, T. Nanocomposites with Polymer Grafted Nanoparticles. *Macromolecules* **46**, 3199–3214 (2013).

27. Jouault, N., Zhao, D. & Kumar, S. K. Role of Casting Solvent on Nanoparticle Dispersion in Polymer Nanocomposites. *Macromolecules* **47**, 5246–5255 (2014).

28. Chao, H., Hagberg, B. A. & Riggleman, R. A. The distribution of homogeneously grafted nanoparticles in polymer thin films and blends. *Soft Matter* **10**, 8083–8094 (2014).

29. Kowacz, M., Marchel, M., Esperança, J. M. S. S. & Rebelo, L. P. N. Ionic liquid-functionalized crystals of barium sulfate: A hybrid organic–inorganic material with tuned hydrophilicity and solid–liquid behavior. *Materials Chemistry and Physics* **160**, 308–314 (2015).

30. Yan, S. *et al.* Surface-grafted silica linked with l-lactic acid oligomer: A novel nanofiller to improve the performance of biodegradable poly(l-lactide). *Polymer* **48**, 1688–1694 (2007).

31. Gao, W. *et al.* Preparation and characterization of BaSO4/poly(ethylene terephthalate) nanocomposites. *Colloids and Surfaces A: Physicochemical and Engineering Aspects* **385**, 181–187 (2011).

32. Jana, S. C. & Jain, S. Dispersion of nanofillers in high performance polymers using reactive solvents as processing aids. *Polymer* **42**, 6897–6905 (2001).

33. upová, M., Martynková, G., yna, S. & Barabaszová, K. Effect of Nanofillers Dispersion in Polymer Matrices: A Review. *Science of Advanced Materials* **3**, 1–25 (2011).

34. Subbiah, R., Veerapandian, M. & Yun, K. S. Nanoparticles: Functionalization and Multifunctional Applications in Biomedical Sciences. *Current Medicinal Chemistry* **17**, 4559–4577 (2010).

35. Thanh, N. T. K. & Green, L. A. W. Functionalisation of nanoparticles for biomedical applications. *Nano Today* **5**, 213–230 (2010).

36. Gillani, R., Ercan, B., Qiao, A. & Webster, T. J. Nanofunctionalized zirconia and barium sulfate particles as bone cement additives. *International Journal of Nanomedicine* **5**, 1–11 (2010).

37. Fang, C. *et al.* Surface functionalized barium sulfate nanoparticles: controlled *in situ* synthesis and application in bone cement. *Journal of Materials Chemistry B* **2**, 1264–1274 (2014).

38. Hernandez, Y. *et al.* Improvement of toughness properties of polypropylene filled with nanobentonite using stearic acid as interface modifier. *Journal of Composite Materials* (2016).

39. Premphet, K. & Horanont, P. Influence of stearic acid treatment of filler particles on the structure and properties of ternary-phase polypropylene composites. *Journal of Applied Polymer Science* **74**, 3445–3454 (1999).

40. Guth, E. Theory of Filler Reinforcement. *Journal of Applied Physics* **16**, 20–25 (1945).

41. Fu, S.-Y., Feng, X.-Q., Lauke, B. & Mai, Y.-W. Effects of particle size, particle/matrix interface adhesion and particle loading on mechanical properties of particulate–polymer composites. *Composites Part B: Engineering* **39**, 933–961 (2008).

42. Kerner, E. H. The Elastic and Thermo-elastic Properties of Composite Media. *Proceedings of the Physical Society. Section B* **69**, 808 (1956).

43. Soares, J. S., Moore, J. E. & Rajagopal, K. R. Theoretical Modeling of Cyclically Loaded, Biodegradable Cylinders, in *Modeling of Biological Materials*, Mollica, F., Preziosi, L. and Rajagopal, K. R. Eds, ed Boston, MA: Birkhäuser Boston, pp. 125–177 (2007).

44. Albano, C., Perera, R., Cataño, L., Karam, A. & González, G. Prediction of mechanical properties of composites of HDPE/HA/EAA. *Journal of the Mechanical Behavior of Biomedical Materials* **4**, 467–475 (2011).

45. Nicolais, L. & Nicodemo, L. Strength of particulate composite. *Polymer Engineering & Science* **13**, 469–469 (1973).

46. Nielsen, L. E. Simple theory of stress-strain properties of filled polymers. *Journal of Applied Polymer Science* **10**, 97–103 (1966).

47. Jancar, J., Dianselmo, A. & Dibenedetto, A. T. The yield strength of particulate reinforced thermoplastic composites. *Polymer Engineering & Science* **32**, 1394–1399 (1992).

48. Wu, W., He, Q. & Jiang, C. Magnetic Iron Oxide Nanoparticles: Synthesis and Surface Functionalization Strategies. *Nanoscale Research Letters* **3**, 397–415 (2008).

49. Abdolmohammadi, S. *et al.* Enhancement of Mechanical and Thermal Properties of Polycaprolactone/Chitosan Blend by Calcium Carbonate Nanoparticles. *International Journal of Molecular Sciences* **13**, 4508–4522 (2012).

50. Mirjalili, F., Chuah, L. & Salahi, E. Mechanical and Morphological Properties of Polypropylene/Nano α-Al(2)O(3) Composites. *The Scientific World Journal* **2014**, 718765 (2014).

51. Chauhan, S. R. & Thakur, S. Effects of particle size, particle loading and sliding distance on the friction and wear properties of cenosphere particulate filled vinylester composites. *Materials & Design* **51**, 398–408 (2013).

52. Yang, J. *et al.* Morphologies, mechanical properties and thermal stability of poly(lactic acid) toughened by precipitated barium sulfate. *Russian Journal of Physical Chemistry A* **89**, 2092–2096 (2015).

53. Zhang, M. Q., Rong, M. Z. & Ruan, W. H. Part II Nanocomposites: Influence of Preparation: Nanoparticles/Polymer Composites: Fabrication and Mechanical Properties A2 - Karger-Kocsis, József, in *Nano- and Mircro- Mechanics of Polymer Blends and Composites*, Fakirov, S., Ed., ed: Hanser, pp. 91–140 (2009).

54. Paul, D. R. & Robeson, L. M. Polymer nanotechnology: Nanocomposites. *Polymer* **49**, 3187–3204 (2008).

55. Lanzer, P. *Mastering Endovascular Techniques: A Guide to Excellence*. Philadelphia, United States: Lippincott Williams and Wilkins, 2006.

56. Imre, B. *et al.* Adhesion and micromechanical deformation processes in PLA/CaSO4 composites. *Carbohydrate Polymers* **89**, 759–767 (2012).

57. Pukánszky, B. Effect of interfacial interactions on the deformation and failure properties of PP/CaCO3 composites. *New Polymeric Materials* **3**, 205–217 (1992).

58. Rothon, R. N. 8. Filled Thermoplastics, in *Particulate-Filled Polymer Composites (2nd Edition)*, ed: Smithers Rapra Technology.

59. Zou, H., Wu, S. & Shen, J. Polymer/Silica Nanocomposites: Preparation, Characterization, Properties, and Applications. *Chemical Reviews* **108**, 3893–3957 (2008).

60. Ahn, S. H., Kim, S. H. & Lee, S. G. Surface-modified silica nanoparticle–reinforced poly(ethylene 2,6-naphthalate). *Journal of Applied Polymer Science* **94**, 812–818 (2004).

61. Bakar, M. & Djaider, F. Effect of Plasticizers Content on the Mechanical Properties of Unsaturated Polyester Resin. *Journal of Thermoplastic Composite Materials* **20**, 53–64 (2007).

62. Lim, H. & Hoag, S. W. Plasticizer effects on physical-mechanical properties of solvent cast Soluplus(R) films. *AAPS Pharm Sci Tech* **14**, 903–10 (2013).

63. Liu, X., Wang, T., Chow, L. C., Yang, M. & Mitchell, J. W. Effects of Inorganic Fillers on the Thermal and Mechanical Properties of Poly(lactic acid). *International Journal of Polymer Science* **2014**, 8 (2014).

64. Khalil, R., Chryss, A. G., Jollands, M. & Bhattacharya, S. Effect of coupling agents on the crystallinity and viscoelastic properties of composites of rice hull ash-filled polypropylene. *Journal of Materials Science* **42**, 10219–10227 (2007).

65. Lee, S.-Y. *et al.* Thermal and Mechanical Properties of Wood Flour/Talc-filled Polylactic Acid Composites: Effect of Filler Content and Coupling Treatment. *Journal of Thermoplastic Composite Materials* **21**, 209–223 (2008).
66. Polu, A. R., Kumar, R., Kumar, K. V. & Jyothi, N. K. Effect of TiO2 ceramic filler on PEG-based composite polymer electrolytes for magnesium batteries. *AIP Conference Proceedings* **1512**, 996–997 (2013).
67. Turcsányi, B., Pukánszky, B. & Tüdős, F. Composition dependence of tensile yield stress in filled polymers. *Journal of Materials Science Letters* **7**, 160–162 (1988).
68. Pukánszky, B., Tüdös, F., Jančař, J. & Kolařik, J. The possible mechanisms of polymer-filler interaction in polypropylene-CaCO3 composites. *Journal of Materials Science Letters* **8**, 1040–1042 (1989).
69. Jong, L. Effect of processing methods on the mechanical properties of natural rubber filled with stearic acid-modified soy protein particles. *Journal of Elastomers and Plastics* **46**, 413–426 (2014).
70. Wu, C. L., Zhang, M. Q., Rong, M. Z. & Friedrich, K. Tensile performance improvement of low nanoparticles filled-polypropylene composites. *Composites Science and Technology* **62**, 1327–1340 (2002).
71. Morel, F., Espuche, E., Bounor-Legaré, V., Persynn, O. & Lacroix, M. Impact of coated calcium carbonate nanofillers and annealing treatments on the microstructure and gas barrier properties of poly(lactide) based nanocomposite films. *Journal of Polymer Science Part B: Polymer Physics* **54**, 649–658 (2016).
72. Hindryckx, F. *et al.* Interfacial adhesion in polyethylene–kaolin composites: Improvement by maleic anhydride-grafted polyethylene. *Journal of Applied Polymer Science* **56**, 1093–1105 (1995).
73. Lin, Y., Chen, H., Chan, C.-M. & Wu, J. High Impact Toughness Polypropylene/CaCO3 Nanocomposites and the Toughening Mechanism. *Macromolecules* **41**, 9204–9213 (2008).
74. Lu, S. *et al.* Is There Light at the End of the Thin-Strut Tunnel? *In Vitro Insights on Strut Thickness Impact on Thrombogenicity in Bioresorbable Stents or Scaffolds* **11**, 714–716 (2018).
75. Koppara, T. *et al.* Thrombogenicity and Early Vascular Healing Response in Metallic Biodegradable Polymer-Based and Fully Bioabsorbable Drug-Eluting Stents. *Circulation: Cardiovascular Interventions* **8**, e002427 (2015).
76. Loza, K. *et al.* Barium sulfate micro- and nanoparticles as bioinert reference material in particle toxicology. *Nanotoxicology* **10**, 1492–1502 (2016).
77. Konduru, N. *et al.* Biokinetics and effects of barium sulfate nanoparticles. *Part Fibre Toxicol* **11**, 55 (2014).
78. Klein, C. L. *et al.* Hazard identification of inhaled nanomaterials: making use of short-term inhalation studies. *Arch Toxicol* **86**, 1137–51 (2012).
79. Schwotzer, D. *et al.* Effects from a 90-day inhalation toxicity study with cerium oxide and barium sulfate nanoparticles in rats. *Part Fibre Toxicol* **14**, 23 (2017).
80. Lämsä, T. *et al.* Biocompatibility of a New Bioabsorbable Radiopaque Stent Material (Ba SO4 Containing Poly-L, D-Lactide) in the Rat Pancreas. *Pancreatology* **6**, 301–305 (2006).
81. Lim, L. T., Auras, R. & Rubino, M. Processing technologies for poly(lactic acid). *Progress in Polymer Science* **33**, 820–852 (2008).
82. Formosa, L. M., Mallia, B. & Camilleri, J. The effect of curing conditions on the physical properties of tricalcium silicate cement for use as a dental biomaterial. *Int Endod J* **45**, 326–36 (2012).

Acknowledgements

Author Contributions

H.Y.A. and Y.H. designed and performed the experiments, conducted data analysis and wrote the manuscript. N.F. and P.W. contributed to the design of the experiments. D.T., W.S.C. and W.S. contributed to the experiment and analysis of the data. W.W. contributed to the finite element analysis of this paper. S.S.V. and Y.H. contributed to the experimental design and manuscript preparation and supervised the overall project. All authors have read and edited the manuscript.

Additional Information

Competing Interests: The authors declare no competing interests.

Publisher's note: Springer Nature remains neutral with regard to jurisdictional claims in published maps and institutional affiliations.